Proceedings of the Canadian Society for Mechanical Engineering International Congress 2021
CSME Congress 2021
June 27-30, 2021, Charlottetown, PE, Canada

FLOW OVER MICRO PILLARS IMMERSED IN A LAMINAR BOUNDARY LAYER: EFFECTS OF MICRO-PILLAR GEOMETRY AND TANDEM INTERACTION

Metin I. Yaras[1], Cagri Metin[1]
[1]Dept. of Mechanical and Aerospace Engineering, Carleton University, Ottawa, Canada

Abstract— The study investigates the flow development in the vicinity and wake of micro pillars mounted on a surface immersed in the inner region of a laminar boundary layer. The investigation is based on the numerical solution of the Navier Stokes equations for incompressible conditions. The height of the micro pillar is shown to significantly affect the tip and base vortices dominating the micro-pillar wake, with this effect extending up to 16 micro-pillar diameters downstream. Tandem installation of two micro pillars with a height-to-diameter ratio of 4.0 eight micro-pillar diameters apart is shown to result in relatively weak aerodynamic interaction of the two micro pillars, with the wake of each micro pillar containing dominant vortical structures of comparable strength.

Keywords- micro pillar wake; tandem micro pillars; vorticity; boundary layers

I. INTRODUCTION

The coherent vortical structures associated with a surface-mounted finite cylinder in a two-dimensional boundary layer are known to be influenced primarily by: the state (turbulent vs. laminar) of the base-surface boundary layer; the height-to-diameter ratio (aspect ratio) of the cylinder; the flow Reynolds number based on the characteristic dimension of the cylinder; and, the thickness of the base-surface boundary layer relative to the cylinder height. These vortical structures can be broadly characterized by three systems: (I) the base vortices and the horseshoe vortex near the cylinder/base-surface junction; (II) vorticity shedding along the height of the cylinder upon separation of the side-surface boundary layer; and, (III) the tip vortex system that is located at the free end of the cylinder. The vorticity source for the horseshoe vortex is the spanwise-oriented vorticity of the undisturbed boundary layer approaching the cylinder along the base surface. This vorticity field concentrates on the windward side of the cylinder under the stagnating influence of the pressure field of the cylinder, with the vorticity vector of the affected fluid particles tilting to develop a streamwise component as they are displaced laterally and vertically from their undisturbed trajectory. The resultant coherent vortical structure at the base of the cylinder is typically referred to as the horseshoe vortex owing to its commonly observed shape [1-4]. On the leeward side of the cylinder, the counter-rotating streamwise-oriented legs of the horseshoe vortex may be accompanied by a second pair of counter-rotating vortices near the base of the cylinder, commonly referred to as the junction or base vortices [1,2,5]. Cylinder aspect ratios larger than a critical value, suggested to be in the 3 to 5 range by Sumner et al. [5], and a relatively thick base-surface boundary layer have been noted to promote the existence of the base vortices [5-7]. The relative strength and characteristics of time-periodic vorticity shedding from the side surfaces of the cylinder depend on the aspect ratio of the cylinder. Below a cylinder aspect ratio of about 2.0 such transient shedding may be suppressed [8], and in the range of 2.0 to 6.0 the periodic shedding is intermittent [9]. At an aspect ratio of 2.5, negligible base surface boundary layer thickness, and a flow Reynolds number based on cylinder diameter of 43,000, Fröhlich and Rodi [10] observed alternating shedding along the lower portion of the cylinder side surface only. Above a critical value of cylinder aspect ratio, which has been observed to depend on the flow Reynolds number and the thickness of the base-surface boundary layer relative to the cylinder height, the boundary layer separating from the side surface of the cylinder rolls asymmetrically or symmetrically from the port and starboard sides into vortical structures in a time-periodic manner that results in the well-known Karman vortex street [9,11]. For low aspect ratios, this vortex shedding appears to be suppressed by the downwash and upwash motions prevailing on the leeward side of the cylinder induced by the vortical structures that exist near the free end and base of the cylinder [1,5,9,11,12]. The vortex system near the free end of the cylinder is somewhat more complex owing to the interaction of the vorticity associated with the top and side surfaces of the cylinder [13]. The geometric discontinuity at the intersection of the top and side surfaces prompts flow separation along the windward edge of the top surface. For cylinders with low aspect ratios, reattachment to the top surface follows [6,7,9,11,14]. Otherwise, the vorticity associated with this separated flow amalgamates into an arch- or mushroom-shaped vortex, with its main portion oriented in the spanwise direction and its legs extending to two focal points on the base surface [6,7,9,10,15,16]. The legs of the arch vortex have been

This study was funded by the Kenneth Molson Foundation.

observed to also merge with a pair of streamwise oriented, counter-rotating tip vortices that emerge from two foci on the rear of the cylinder near the leeward edge of the cylinder top surface [10]. The tip vortices were also identified as the dominant vortical structures on the free end of the cylinder by Hain et al. [14].

The surface-mounted cylinder configurations that have been studied to date have tended to place the free end of the cylinder either in the upper portion or beyond the edge of the boundary layer. In a two-dimensional boundary layer developing under zero or favourable streamwise pressure gradients, majority of the boundary-layer vorticity is confined to the inner region of the boundary layer. Based on the flow physics reviewed in the foregoing, placing the free end of the cylinder within this high-vorticity region may yield dynamics that deviate from the trends observed for cylinders where the undisturbed-flow vorticity near the free end of the cylinder is either low or zero. A computational study recently conducted by the present authors for such a configuration [17] demonstrated a unique wake development for a surface-mounted micro pillar immersed in the inner region of the surface boundary layer. The present study builds on this initial work by investigating variations in the micro pillar dimensions and a configuration involving two micro pillars in tandem. This scope of the present study was established to enable its support of a planned future study to passively control turbulence in turbulent boundary layers.

II. Computational Model

The computational domain and boundary conditions for the single and tandem micro pillar configurations are illustrated in Fig. 1. In both instances, the domain is conservatively sized to allow for the flow field in the vicinity of each micro pillar and its wake to develop without any artificial influence by the imposed boundary conditions. The positioning of the outflow boundary relative to the location of the micro pillar is also driven by the need to have sufficient distance for the wake region to develop downstream of the micro pillar. The domain height is set to over three times the inflow boundary-layer thickness and four times the length of the domain. These choices ensure absence of a streamwise pressure gradient in the undisturbed freestream. The computational domain for the shorter micro pillar (H/D=2.5) of the study is based on the same dimensions as those illustrated in Fig. 1.

The laminar-flow velocity profile at the inflow boundary is at a Reynolds number based on momentum thickness of 900. The present study is a precursor to an investigation of micro pillars for passive control of turbulence in turbulent boundary layers. Accordingly, the present study is set up with a background boundary layer of a vorticity distribution that approximates that of a turbulent boundary layer. Specifically, the velocity profile corresponds to that of an equilibrium turbulent boundary layer developing under zero streamwise pressure gradient. When normalized by the local wall shear stress at the axial location of the micro pillar and the fluid viscosity, the micro-pillar diameter has a value of D^+=18. For the two micro-pillar heights of H/D =4.0 and 2.5 of this study, the corresponding normalized micro-pillar height is H^+=72 and 45, respectively.

The spatial grid mapped into each of the computational domains is based on a block-structured grid layout of hexahedral cells. For a well-controlled distribution of the grid cell size, the domain is subdivided into multiple blocks in the streamwise, spanwise and wall-normal directions as shown in Fig. 2 for the single and tandem micro-pillar configurations. The smallest grid cells with a size of 0.01D are located in the vicinity of the micro-pillar. This, together with the mild rate of spatial gradients in the cell sizes as illustrated by the R parameter in Fig. 2, results in a total grid-cell count of 4.6 million in the single-micro-pillar domain, and 7.6 million in the tandem-micro-pillar domain. These spatial grids yield a very conservative spatial resolution of the flow field. This was confirmed through a grid-sensitivity analysis for each configuration. The time-step size normalized by U_{ref} and D is set to 0.002. This time increment yields a Courant number value of less than 0.5 for any of the grid cells in the domain. This is sufficient for numerical stability and is also suitable for resolving possible time-periodic shedding of vorticity in the wake of the micro pillar.

The commercial software package ANSYS CFX 13.0 is used to solve the continuity and momentum equations governing the incompressible fluid flow. The authors' research group has used and validated the solution algorithm of this software extensively in direct numerical simulations of attached and separated shear layers in transitioning and turbulent states [18]. The governing equations are spatially discretized using a finite volume approach. Spatial derivatives are evaluated using a spatial interpolation scheme that is equivalent to second-order centered-differencing for the diffusion term, and a blend of first-order of upwind and second-order centered differencing for the convection term. Second-order Euler backward differencing is used for temporal derivatives. Benchmark simulations performed by the authors' research group have shown a root-mean-square normalized residual value on the order of 10^{-5} to be adequate for satisfactory convergence.

III. Results and Discussion

The Reynolds number based on the micro-pillar diameter, D, and the undisturbed boundary layer velocity at the streamwise (x) location of the single micro pillar at z=H distance from the base surface is 125. Given the wall-normal velocity gradient, this Reynolds-number value would be 68 if it were based on the velocity spatially averaged over the height of the micro pillar rather than the value at z=H. A 2D (i.e. infinitely long) cylinder in uniform cross flow at these flow Reynolds number values falls in the 40-150 Reynolds-number range for which the cylinder would experience transient alternating vortex shedding from its starboard and port sides

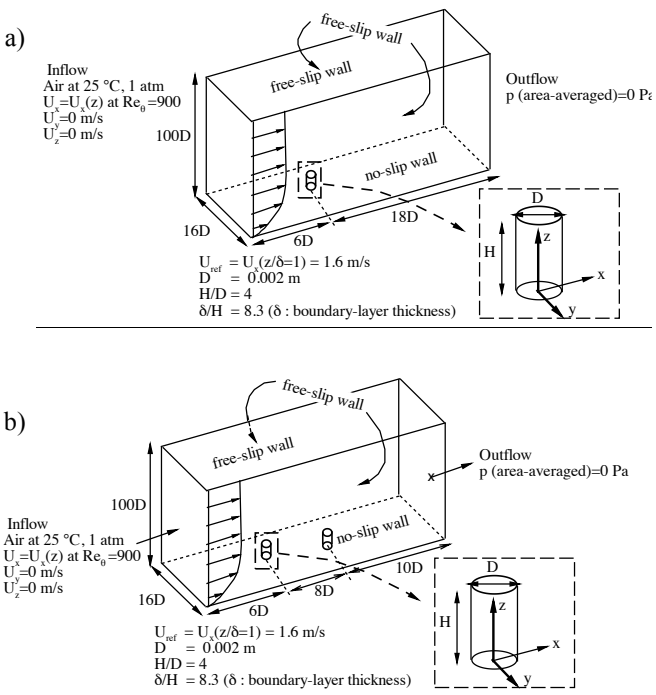

Figure 1 Computational domain and boundary conditions: a) single micro pillar; b) two micro pillars in tandem.

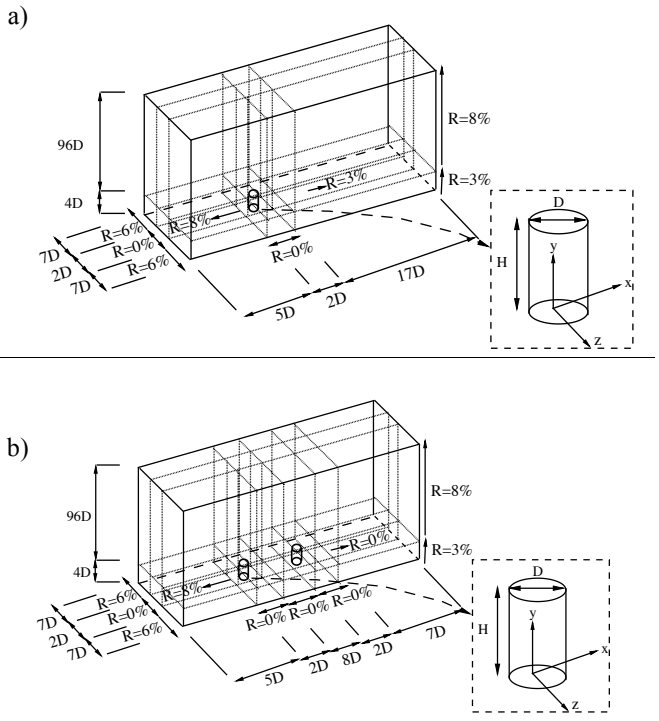

Figure 2 Grid-block topology (R: grid-cell growth rate): a) single micro pillar; b) two micro pillars in tandem.

to produce the well-known Karman vortex street. The present simulation results and those in the precursor study [17] indicate a steady flow field for all the configurations considered. The aspect ratio of the micro pillar may affect this outcome. A height-to-diameter ratio of 2.0 has been suggested in the published literature as the threshold below which periodic shedding in the wake is suppressed. The H/D ratios of 2.5 and 4 considered in the present study are both higher than this threshold. It is therefore interesting to observe suppression of the absolute instability mechanism driving the periodic shedding of vortices. The micro pillars of the present study are placed in a cross-flow with a velocity gradient that is significantly higher along the full height of the micro pillar than the cross-flow conditions considered in the published literature. It may therefore be argued that this gradient plays a significant role in suppression of periodic shedding from the micro pillar. Analysis of the flow field around the micro pillar and its wake as presented in the recent precursor study [17] with reference to Fig. 3 helped to further explore this cause-and-effect relationship. Part (a) of the figure presents the limiting flow streamlines on the top and side surfaces of the micro pillar, which are in essence skin friction lines. Part (b) presents the skin friction lines on the base surface (z=0 plane) and the streamlines on the y=0 plane together with the static pressure distributions in these planes illustrated as a flood plot of the static pressure coefficient defined as $(P-P_{ref})/0.5\rho U_{ref}^2$, where the reference condition corresponds to the undisturbed freestream condition. The plotted range for this pressure coefficient is based on the pressure range realized within the x, y and z bounds of the plot. Part (c) presents isosurfaces of the second invariant of the velocity gradient tensor (Q). The isosurfaces correspond to a nondimensional Q value of 0.00375, for which the reference velocity and the micro-pillar diameter are used for normalization.

The surface skin-friction-line pattern on the micro pillar suggests the presence of several singular points, which develop at surface locations where the wall shear stress or the surface vorticity becomes identically zero. Conventionally such singular points are identified as either saddle points or nodes, and nodes are further subcategorized as either nodal points or foci of attachment or separation [19]. At a nodal point, all but one of the skin friction lines converging to that point become tangent to a single line passing through the point. Whether the lines are directed towards or away from the point depends on whether the nodal point corresponds to flow separation or attachment, respectively. A focal point differs from a nodal point in that the skin friction lines do not have a common tangent at such a singular point; instead, they converge at that point in a spiral pattern. For example, a vortex connecting with a surface would yield a focal point. At a saddle point, only two skin friction lines intersect, with the skin friction directed towards the point on one of the lines, and away from it on the other. All other skin friction lines in the vicinity avoid this point, with the two intersecting skin friction lines in effect acting as barriers for these remaining lines. With these definitions, identification of nodal, focal and saddle

points on the micro-pillar surface shed considerable light on the flow field around the micro pillar.

In Fig. 3a, the front view of the micro pillar shows a nodal point in the y=0 plane, $1/4^{th}$ of micro pillar height away from the top surface of the micro pillar. A saddle point forms in the same plane at the base of the micro pillar. In the precursor study [17], these points were shown to be the unique result of the micro pillar being immersed in a flow of significant gradient in streamwise velocity. For the shorter micro pillar (H/D=2.5), these points are noted at very similar relative positions along the height of the micro pillar, as illustrated in Fig. 4a. Accordingly, the starting conditions for the development of a new boundary layer over the side surface of the micro pillar is quite similar for the two micro pillars. This boundary layer separates at some point along the perimeter of the micro pillar, as is seen in the side view in Figs. 3a and 4a. The location of the point of separation varies along the height of the micro pillar in a very similar manner for the shorter and taller micro pillars. The delay in separation as the base of the micro pillar is approached is consistent with the reduction in the local flow Reynolds number with proximity to the base surface, as affected by the velocity gradient in the cross flow.

The spiraling pattern of skin-friction lines observed on the separation line near the base surface of both the taller and shorter micro pillars is a focal point associated with termination of the base vortex on the micro pillar surface. This vortex rotating counter-clockwise when viewed from downstream and its counterpart of opposite sense of rotation on the starboard side are readily evident in the wake of the taller micro pillar in Fig. 3c. This pair of base vortices is noted to be significantly weaker for the shorter micro pillar in Fig. 4c. As was demonstrated in the precursor study [17], the source of vorticity for the base vortices is the boundary layer developing on the micro-pillar side surface. The vorticity of this boundary layer develops a streamwise (x) component due to the cross-flow velocity gradient along the height of the micro pillar. Given this mechanism, the notably reduced surface area of the shorter micro pillar relative to the taller one explains the reduced amount of total vorticity available for the base vortices. The upwash induced by the notably stronger base vortices in the wake of the taller micro pillar, which is visible in the streamline patterns in the geometric symmetry plane on the leeward side of the micro pillar in Fig. 3b, results in their movement away from the base surface with streamwise distance, as illustrated in Fig. 5. This effect is notably diminished for the weaker base vortices of the shorter micro pillar. As was described in the precursor study [17], the tip vortices labeled in Figs. 3 and 4 are also sourced by the vorticity of the boundary layer developing on the side surface of the micro pillar. These vortices are observed to be of comparable strength to the base vortices in the wake of the shorter micro pillar, but notably weaker than the base vortices in the wake of the taller micro pillar. Their sense of rotation is opposite of those of the base vortices, and accordingly they induce downward motion upon each other. The elevation variation of these vortices with streamwise distance, shown in Fig. 5 confirms this, with the extent of this motion being consistent with the relatively low strength of these vortices.

The streamwise rate of diffusion of the base and tip vortices is observed through the peak value of the streamwise (x) component of vorticity in Fig. 6. The diffusion rate is noted to be significantly higher for the stronger base vortices of the taller micro pillar, with their peak vorticity reaching a magnitude that is comparable to that of the tip vortices of this micro pillar at 16 diameters downstream of the micro pillar. It is further observed that at this streamwise location these peak vorticity values are also comparable to those observed in the wake of the shorter micro pillar. If such surface-mounted micro pillars are to be used for passive control of turbulence in a turbulent boundary layer, the wake vortices of the micro pillar must be sufficiently strong to affect the local turbulence of the boundary layer. Of the two micro pillars considered in the present study, the taller may be suitable for this effect. Given that the tip and base vortices are both sourced by the side-wall boundary layer of the micro pillar, they may be further strengthened by increasing the micro pillar height. Optimizing the micro pillar dimensions in this context would also have to involve the effect of the frontal area of the micro pillar on its aerodynamic drag. For surface-mounted micro pillars to have a sustained effect on boundary-layer turbulence, multiple micro pillars must be mounted onto the surface in a suitable pattern. Streamwise rows of micro pillars of strategically chosen streamwise and spanwise spacings may be a promising configuration to consider based on the well-known fundamental layout of small-scale vortical structures in wall turbulence [18]. In such a micro-pillar layout, the streamwise spacing of the micro pillars should be chosen such that their streamwise proximity to each other does not adversely affect their individual function of generating strong wake vortices, while at the same time they are sufficiently close to each other to realize continuous influence on turbulence eddies as these eddies convect along the rows of micro pillars. Based on the trends in Fig. 6, streamwise spacing the taller micro pillar by about 8 diameters may cater to these objectives. At this streamwise distance, the wake vortices of the upstream micro pillar are still relatively strong, yet they may have diffused sufficiently to not affect the aerodynamics of the downstream micro pillar to a significant extent. A simulation was performed for this configuration, the results of which are presented in Figs. 7 and 8. While the wake structures of the two micro pillars display visible differences, they appear to develop wake vortices of comparable strength and trajectories. This favourable comparison is particularly interesting in light of the considerable differences observed in the surface streamlines of the two micro pillars (Fig. 7a) and the streamlines in the geometric symmetry plane of the wake (Fig. 7b). Further optimization of the streamwise spacing of the micro pillar requires interpretation of these patterns, which will be reported in a subsequent paper.

IV. CONCLUSIONS

Numerical simulations are performed of the laminar flow around micro-pillars immersed in the inner region of a zero-streamwise-presure-gradient boundary layer on a flat surface.

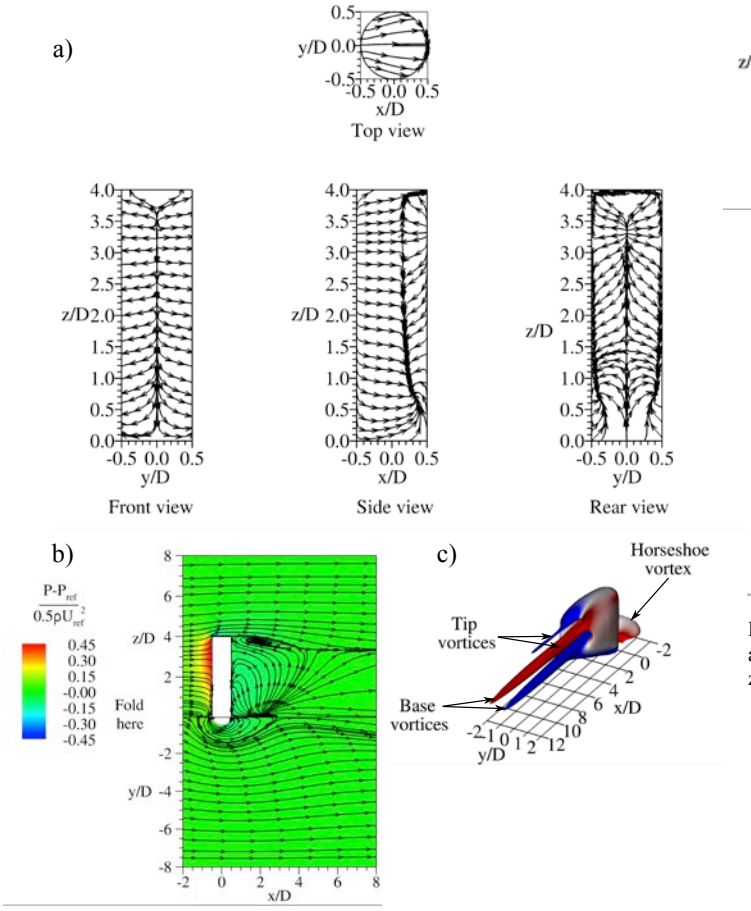

Figure 3 Flow field in the vicinity and wake of the micro pillar with H/D=4.0: a) micro-pillar surface streamlines; b) pressure field and streamlines in y=0 & z=0 planes; c) Q=0.00375 isosurfaces.

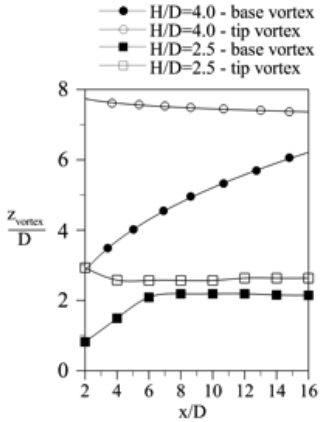

Figure 5 Streamwise variation of wall-normal distance of the base and tip vortices.

The micro pillars are exposed to the portion of the boundary layer where the vorticity magnitude is relatively the highest. The micro-pillar wake is observed to be steady, dominated by

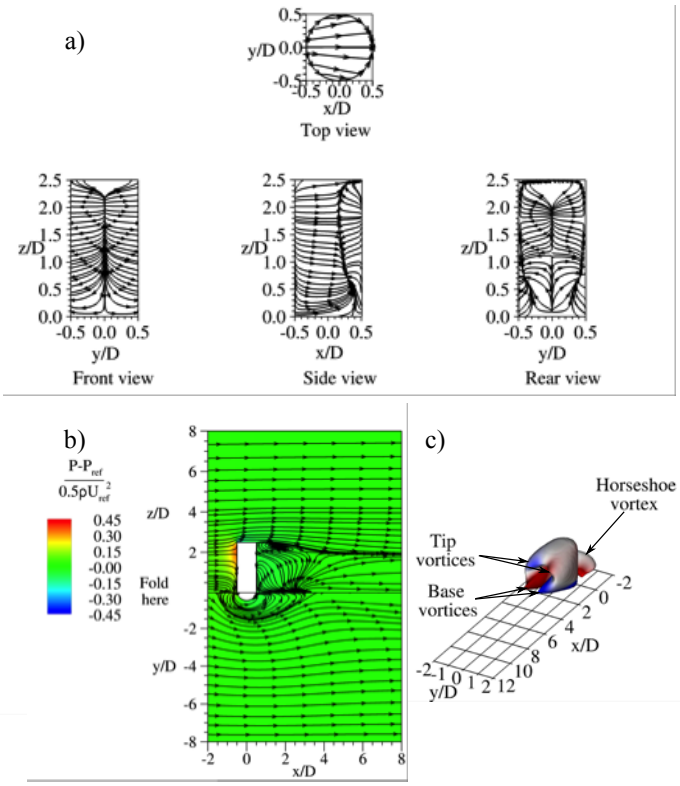

Figure 4 Flow field in the vicinity and wake of the micro pillar with H/D=2.5: a) micro-pillar surface streamlines; b) pressure field and streamlines in y=0 & z=0 planes; c) Q=0.00375 isosurfaces.

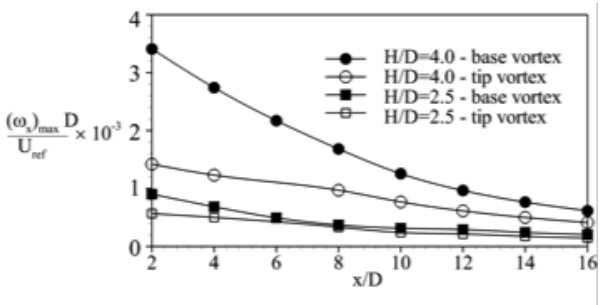

Figure 6 Streamwise variation of peak streamwise vorticity in the base and tip vortices.

a pair of base vortices and a pair of tip vortices. For the taller micro pillar (H/D=4.0), the base vortices are stronger than the tip vortices, and both pair of vortices follow a streamwise trajectory dictated by their mutually induced wall-normal motions. Both pairs of vortices are observed to be significantly weakened when the micro-pillar height is reduced (H/D=2.5). This trend is consistent with the observation that the vorticity for both pair of vortices originate from the side-wall boundary layer of the micro pillar. In tandem installation of two of the taller micro pillars, streamwise spacing of eight micro-pillar diameters is shown to yield relatively weak aerodynamic interaction between the two micro pillars. Specifically, the wake of the upstream micro pillar retains the features of the isolated micro-pillar configuration, and the wake of the downstream micro pillar contains vortices of strength and size that appear comparable to those of the upstream micro pillar.

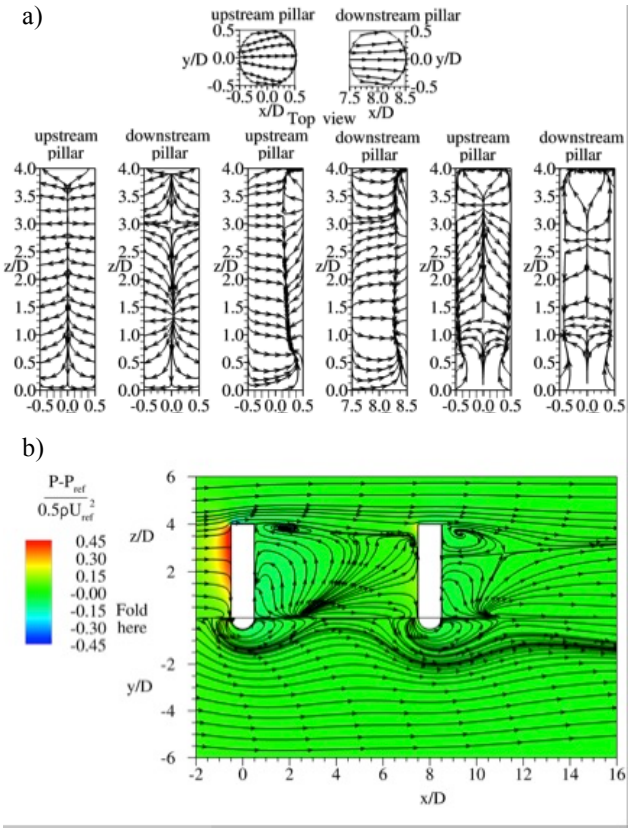

Figure 7 Flow field in the vicinity and wake of the tandem micro pillars: a) micro-pillar surface streamlines; b) pressure field and streamlines in y=0 & z=0 planes.

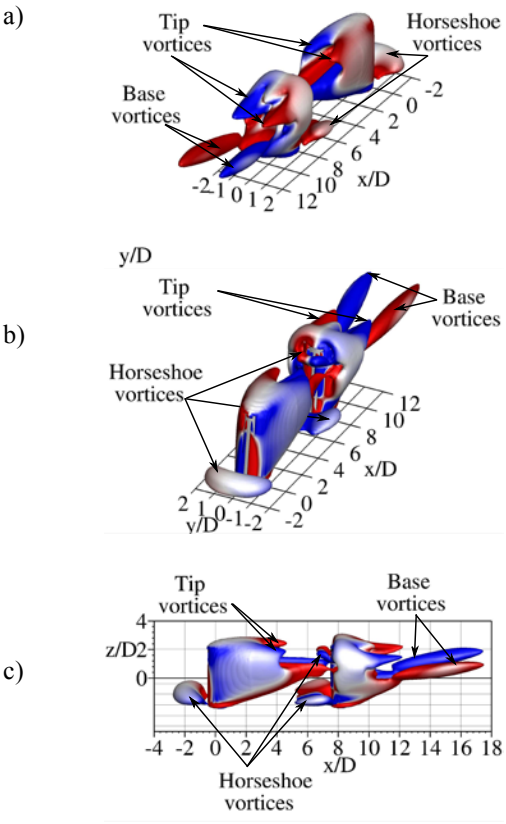

Figure 8 Flow field in the vicinity and wake of the tandem micro pillars observed through the Q=0.00375 isosurfaces: a) view of the wakes; b) view of the windward side of the micro pillars; c) viewed from the y coordinate direction.

REFERENCES

[1] G.D. Donnert, M. Kappler and W. Rodi, "Measurement of tracer concentration in the flow around finite-height cylinders," J. of Turbulence, (8), N33, 2007.

[2] A. Sau, R.R. Hwang, T.W. Sheu and W.C. Yang, "Interaction of trailing vortices in the wake of a wall-mounted rectangular cylinder," Physical Review E, 68(5), 056303, 2003.

[3] C. Lin, P.H. Chiu, S.J. Shieh, "Characteristics of horseshoe vortex system near a vertical plate–base plate juncture," Experimental Thermal and Fluid Science, 27(1), pp. 25-46, 2002.

[4] C.J. Baker, "The laminar horseshoe vortex," J. of Fluid Mechanics, 95(2), pp. 347-367, 1979 .

[5] D. Sumner, J.L. Heseltine and O.J.P. Dansereau, "Wake structure of a finite circular cylinder of small aspect ratio," Experiments in Fluids, 37(5), pp. 720-730, 2004.

[6] R.J. Pattenden, S.R. Turnock and X. Zhang, "Measurements of the flow over a low-aspect-ratio cylinder mounted on a ground plane," Experiments in Fluids, 39(1), pp. 10-21, 2005.

[7] R.J. Pattenden, N.W. Bressloff, S.R. Turnock and X. Zhang, "Unsteady simulations of the flow around a short surface-mounted cylinder," J. for Num. Methods in Fluids, 53, pp. 895-914, 2007.

[8] T. Okamoto and M. Yagita, "The experimental investigation on the flow past a circular cylinder of finite length placed normal to the plane surface in a uniform stream," Bull. JSME 16, 1973.

[9] T. Kawamura, M. Hiwada, T. Hibino, I. Mabuchi and M. Kumada, "Flow around a finite circular cylinder on a flat plate: cylinder height greater than turbulent boundary layer thickness," Bulletin of JSME, 27(232), pp. 2142-2151, 1984.

[10] J. Fröhlich and W. Rodi, "LES of the flow around a circular cylinder of finite height," Int. J. of Heat and Fluid Flow, 25(3), pp. 537-548, 2004.

[11] D. Sumner, "Flow above the free end of a surface-mounted finite-height circular cylinder: a review," J. of Fluids and Structures, 43, pp. 41-63, 2013.

[12] H. Wang, Y. Zhou, C. Chan and T. Zhou, "Momentum and heat transport in a finite-length cylinder wake," Experiments in Fluids, 46(6), pp. 1173-1185, 2009.

[13] Z. Hosseini, J.A. Bourgeois and R.J. Martinuzzi, "Large-scale structures in dipole and quadrupole wakes of a wall-mounted finite rectangular cylinder," Experiments in Fluids, 54(9), pp. 1595-1610, 2013.

[14] R. Hain, C.J. Kähler and D. Michaelis, "Tomographic and time resolved PIV measurements on a finite cylinder mounted on a flat plate," Experiments in Fluids, 45(4), pp. 715-724, 2008.

[15] S. Krajnović, "Flow around a tall finite cylinder explored by large eddy simulation," J. of Fluid Mechanics, 676, pp. 294-317, 2011.

[16] G. Palau-Salvador, T. Stoesser, T., J. Fröhlich, M. Kappler and W. Rodi, "Large eddy simulations and experiments of flow around finite-height cylinders," Flow, Turb. and Comb., 84(2), 239, 2010.

[17] Yaras, M.I. and Metin, C., "Numerical Study of the Fluid Dynamics of a Micro Pillar Immersed in a Laminar Boundary Layer," Proceedings of the Canadian Society for Mechanical Engineering Int. Congress 2020.

[18] J. Brinkerhoff and M.I. Yaras, "Numerical investigation of the generation and growth of coherent flow structures in a triggered turbulent spot," J. of Fluid Mechanics 759, pp. 257–294, 2014.

[19] M. Tobak and D.J. Peake, "Topology of three-dimensional separated flows," Ann. Rev. Fluid Mech., Vol. 14, pp. 61-85, 1982